PCCP

# Gamma radiation-induced defects in KCl, $MgCl_2$, and $ZnCl_2$ salts at room temperature

| | |
|---|---|
| Journal: | *Physical Chemistry Chemical Physics* |
| Manuscript ID | CP-ART-02-2021-000520.R2 |
| Article Type: | Paper |
| Date Submitted by the Author: | 15-Apr-2021 |
| Complete List of Authors: | Ramos-Ballesteros, Alejandro; University of Notre Dame, Radiation Laboratory<br>Gakhar, Ruchi; Idaho National Laboratory, Pyrochemistry and Molten Salt Systems Department<br>Horne, Gregory; Idaho National Laboratory, Center for Radiation Chemistry Research<br>Iwamatsu, Kazuhiro; Brookhaven National Laboratory Department of Chemistry<br>Wishart, James; Brookhaven National Laboratory Department of Chemistry<br>Pimblott, Simon M.; Idaho National Laboratory, Nuclear Science & Technology<br>Laverne, Jay A; University of Notre Dame Research, Radiation Laboratory |
| | |

ARTICLE

# Gamma radiation-induced defects in KCl, $MgCl_2$, and $ZnCl_2$ salts at room temperature

Received 00th January 20xx,
Accepted 00th January 20xx

DOI: 10.1039/x0xx00000x

**Alejandro Ramos-Ballesteros*[a], Ruchi Gakhar[b], Gregory P. Horne[c], Kazuhiro Iwamatsu[d], James F. Wishart[d], Simon M. Pimblott[e], and Jay A. LaVerne[a, f]**

Room temperature post-irradiation measurements of diffuse reflectance and electron paramagnetic resonance spectroscopies were made to characterize the long-lived radiation-induced species formed from the gamma irradiation of solid KCl, $MgCl_2$, and $ZnCl_2$ salts up to 100 kGy. The method used showed results consistent with those reported for electron and gamma irradiation of KCl in single crystals. Thermal bleaching of irradiated KCl demonstrated accelerated disaggregation of defect clusters above 400 K, due to decomposition of $Cl_3^-$. The defects formed in irradiated $MgCl_2$ comprised a mixture of $Cl_3^-$, *F*-centers, and monovalent Mg cations ($Mg^+$) associated as M-centers. Further, Mg metal cluster formation was also observed at 100 kGy, in addition to accelerated destruction of *F*-centers above 20 kGy. Irradiated $ZnCl_2$ afforded the formation of $Cl_2^-$ due to its high ionization potential and crystalline structure, which decreases recombination. The presence of aggregates in all cases indicates the high diffusion of radicals and the predominance of secondary processes at 295 K. Thermal bleaching studies showed that chloride aggregates stability increases with the ionization potential of the cation present. The characterization of long-lived radiolytic transients of pure salts provides important information for the understanding of complex salt mixtures under the action of gamma radiation.

## Introduction

Molten Salt Reactors (MSRs) are a class of Next Generation Nuclear Plant (NGNP) in which the primary coolant, or even the fuel itself (liquid-fueled), is a molten-salt mixture. MSR concepts promise useful features such as high temperatures, low-pressure cooling systems, enhanced intrinsic safety, and greater thermal-to-mechanical efficiencies than, for example, light water reactors.[1, 2] In order to ensure reliable MSR operation it is important to understand the interactions of ionizing radiation with different salts, decay products, and nuclear materials.[3] Radiation-induced radicals and reactive species could significantly impact corrosion, metal ion speciation, and steady-state equilibria in the mixture, all of which, to the possible detriment of reactor performance and durability.

Spectrophotometric analysis of transients in molten salts can be performed at steady-state (equilibrium) or in real time with pulse radiolysis (short-lived),[4, 5] but the alternative approach of solid-state radiolysis can complement the study of long-lived trapped radiolytic transients and ultimately provide information on their speciation, kinetics, and decay mechanisms (photolytic and thermal bleaching).[6] The relative stability of these trapped transients allows facile study of frozen, vitrified, or powdered irradiated salts, at longer measuring times (>$10^{-3}$ s) and under milder experimental conditions, adding flexibility to the suite of analytical techniques that can be employed.[7] Solid-state radiolysis studies in conjunction with pulse radiolysis in molten salts and irradiation in steady state at high temperatures, can provide vital information difficult to obtained at extreme environments, for instance, coordination geometries and oxidation states of divalent cations in irradiated chlorides.

Trapped radiolytic transients (contained or associated to defects) represent the initial species generated upon the interaction of ionizing radiation with a salt medium, as there is little interference from subsequent diffusion and reaction kinetic processes. Consequently, understanding the nature of these initial species at different temperatures, doses, and types of radiation, supports the development of models for more complex salt systems at higher temperatures.

Ionizing radiation-induced defects in alkali halides (AH) have been widely studied since the 1940s, due to their characteristic absorption features in the UV-Vis spectrum.[3] Electron, X- or γ-irradiated crystals of alkali fluorides,[8, 9] iodides,[10, 11] bromides,[12, 13] chlorides[14, 15] and mixtures thereof[16] have served as model systems for understanding of phenomena in solid-state physics.[17] As a result, nowadays it is known that factors such as

[a] *Notre Dame Radiation Laboratory, University of Notre Dame, Notre Dame, Indiana 46556.*
[b] *Pyrochemistry and Molten Salt Systems Department, Idaho National Laboratory, Idaho Falls, ID 83415.*
[c] *Center for Radiation Chemistry Research, Idaho National Laboratory, Idaho Falls, ID 83415.*
[d] *Chemistry Division, Brookhaven National Laboratory, Upton, NY 11973.*
[e] *Nuclear Science User Facilities, Idaho National Laboratory, Idaho Falls, 1955 N. Fremont Ave. ID 83415.*
[f] *Department of Physics, University of Notre Dame, Notre Dame, Indiana 46556.*
† Corresponding author: aramosb2@nd.edu.
Electronic Supplementary Information (ESI) available: Thermal bleaching analysis for $MgCl_2$. See DOI: 10.1039/x0xx00000x

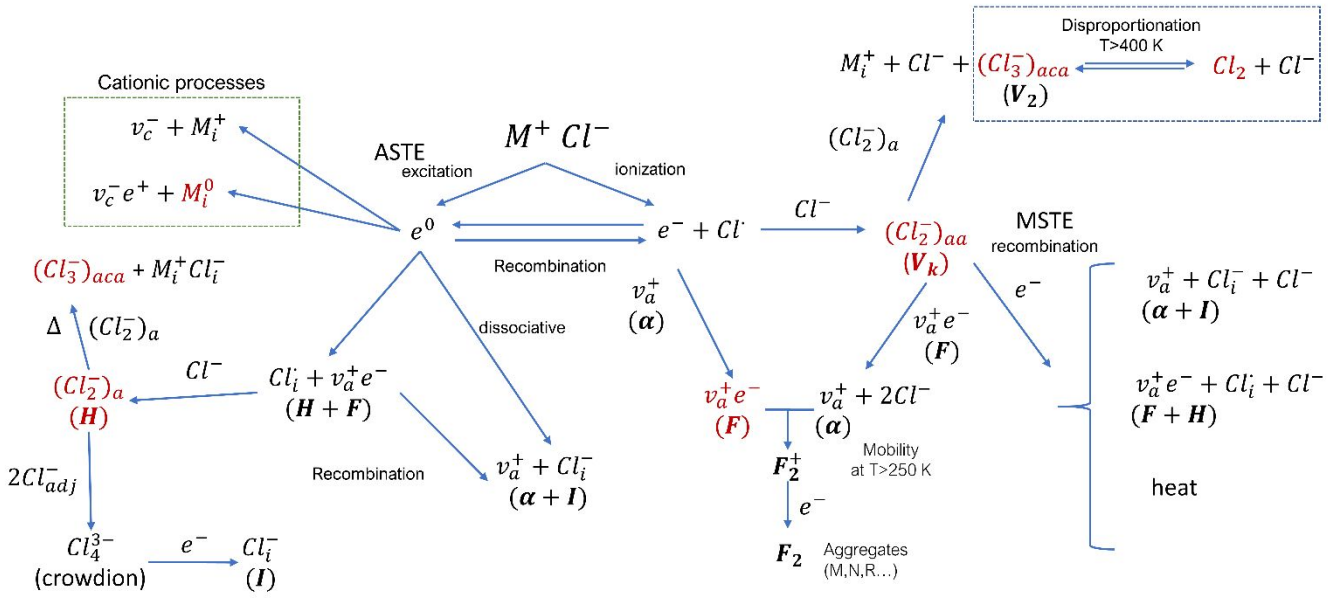


**Fig. 1**. General scheme for the main transient and persistent species induced by ionizing radiation on solid monovalent chlorides. $e^0$ = exciton; $v_a^+$ = anion vacancy; $Cl_i^-$ = interstitial chloride; $e^-$ = electron; $Cl^\cdot$ = hole; $v_a^+ e^-$ = F-center (trapped electron); $Cl_i^\cdot$ or $(Cl_2^-)_a$ = *H*-center (interstitial halogen atom); $(Cl_2^-)_{aa} = V_k$-center; $(Cl_3^-)_{aca} = V_2$-center; $v_c^-$ = cation vacancy; $M_i^+$ = interstitial cation; $v_c^- e^+$ = trapped hole in a cation vacancy (theoretical); $M_i^0$ = interstitial metal atom; ASTE atomic self-trapped exciton and MSTE= molecular self-trapped exciton

unit cell; lattice constant; coordination; charge and ionization potential of the constituent cation and halide; extent of impurities;[18, 19] and irradiation conditions as temperature,[20, 21] radiation quality, and absorbed dose; determine the type and concentration of defects induced by ionizing radiation. Despite all the latter variables, the types of defects detected and characterized in solid salt systems consist of electrons and holes trapped in the lattice as either isolated species (*F*-, *F*'-, and *V*-centers) or as aggregates ($F_2$-, $F_3$-, $F_4$- or $X_n^-$ centers).[22, 23] The definition of a defect is the disruption of a regular pattern within a crystalline arrangement. But when we generate defects with ionizing radiation, the defects that interrupt the pattern can contain transient species such as $Cl_2^-$, $Cl_3^-$, $Zn^+$, $Mg^+$ and electrons trapped in negative vacancies as in F-centers. These defects are actually long-lived trapped transients that are destroyed by heating well below the melting point, or with UV-Vis light. Thermal studies showed in some cases that as little as 20 ° C above room temperature is sufficient to generate decay. Hence, we use the word "transients" to refer to various ions or molecules that are contained or associated with some absorption bands in the spectra shown below.

Data regarding alkaline earth or transition metals halides, although existing, is more limited. Due to their potential applications in scintillation detectors and semiconductors, studies have been conducted on fluorides and iodides of alkaline earth metals such as Ca, Sr, Mg, and Ba, exposed to X-rays, electrons, or gammas,[24-26] but few regarding chlorides. Unlike AH, the presence of divalent cations generates not only *F*-centers and colloidal metal, but defects involving monovalent cations with different coordinations and symmetries whose abundance will be determined by the ionization potential, coordination geometry, and packaging. The primary and secondary processes in salts with divalent cations are similar to AH, although with some essential differences, for instance, in AH it is known through low-temperature radiolysis studies that the primary transients are neutral Frenkel defect pairs (*F*- and *H*- centers); while in halides of divalent cations, charged FD pairs (anionic vacancies (α) and interstitial halides ($I$)) are produced.[3] The newly formed anion vacancies can capture an electron from another ionization process to generate *F*-centers, and interstitial ions ($I$-centers) begin to aggregate to form $X_3^-$ and colloidal metal ($M^0$). Proposed models about the growth of aggregates in AH and the possible structures of dislocation loops can be reviewed elsewhere.[27] Figure 1 shows a general scheme of solid-state radiolysis in AH.

Sibley et al[28] conducted electron and gamma irradiation studies on $MgF_2$ crystals varying temperature. They found a similar behavior to the coloration in KCl with respect to temperature, with peaks at 260, 370, and 400 nm, which they associated the first with *F*-centers and the last two with *M*-centers of different geometries. One of the main differences stated with respect to AH is the formation of interstitial aggregates instead of H centers. In 1991 Nakagawa[29] carried out a more detailed analysis of the symmetry of the M-centers induced by neutron irradiation, finding peaks at 300, 325, 355 and 400 nm at room temperature.

The only previous study regarding the irradiation of $MgCl_2$ in single crystals was carried out by Kinno and Onaka in 1982,[30] where commercial and recrystallized single crystals were irradiated with X-rays and gammas at different temperatures. The absorption spectra showed two peaks at 285 and 370 nm. Kinno concluded that the peak at 370 corresponds to *F*-centers, without assigning the one found at a higher wavelength. The EPR spectrum showed a wide resonance line (similar to KCl) without angular dependence, with g =2.0009 ± 0.0009 which they assigned to *F*-center.

Zinc halides have only been studied as fluorides and as a dopant in alkaline earth metal crystals, but there are no reported solid-state radiolysis studies for chlorides. Only one doctoral dissertation carried out by Butler in 1972[31] was found where absorption spectra for $MgF_2$ and $ZnF_2$ were obtained, making a comparison between systems since they share coordination numbers, although it is not the same crystalline structure. Butler found peaks at 350 nm and 240 nm, associating the longer wavelength absorption to $F_2$-centers by analogy to $MgF_2$, although without conclusive evidence for such assignment.

To this end, we present absorption and EPR spectra for KCl, $MgCl_2$, and $ZnCl_2$ powders gamma-irradiated up to 100 kGy absorbed dose. The analysis and comparison of monovalent (KCl) and divalent ($MgCl_2$ and $ZnCl_2$) chlorides, with different coordination environments (octahedral for KCl and $MgCl_2$, and tetrahedral for $ZnCl_2$) and ionization potentials, facilitates correlation between the abundance of transients, their stability, and reactivity. Irradiation and measurement were carried out at room temperature, with subsequent thermal bleaching to monitor decay rates. Diffuse reflectance spectroscopy was performed with a crafted polymeric holder at Θ=45°, and EPR in the X-band range for radical species.

## Methodology

### Materials

Magnesium chloride ($MgCl_2$, 99.9% anhydrous, MilliporeSigma) and zinc chloride ($ZnCl_2$, >98% anhydrous, Alfa-Aesar) were procured and purified by distillation at Oak Ridge National Laboratory (ORNL), as previously described.[32] Potassium chloride (KCl, 99.998% ultra-dry, Alfa-Aesar) was used without further purification.

### Sample preparation

Both distilled and anhydrous commercial grade salts were crushed to fine powder using an agate pestle and mortar, and subsequently loaded (0.0902-0.1762 ± 0.0002 g) and flame-sealed in synthetic quartz glass tubes (Suprasil®) under argon atmosphere.

### Gamma Irradiations

Gamma irradiations were performed at room temperature (~298 K) using a Shepherd 109 Cobalt-60 irradiator unit at the University of Notre Dame Radiation Laboratory. Samples were irradiated at a dose rate of 72.4 Gy $min^{-1}$ as determined by Fricke dosimetry[33] corrected for cobalt-60 decay ($^{60}Co$, $t_{1/2}$ = 5.27 years, $E_{\gamma1}$ = 1.17 MeV and $E_{\gamma2}$ =1.33 MeV). The employed dose rate did not produce macroscopic heating, or at least the equilibrium of destruction/formation of *F*-centers remains positive for coloration at the end of the irradiation. Spectra were obtained 20 sec after reaching the desired absorbed dose. The samples were kept in the dark during the transfer periods between measurements and irradiations to avoid excessive bleaching from ambient light.

### Thermal bleaching

After irradiation at 100 kGy, the rate of change in absorption intensity was monitored for the observed defects at increasing temperatures. Thermal bleaching was achieved by isochronous annealing (10 min) in an oven at several temperatures from 298 to 440 K. After heating, tubes were quenched for 2 min in water prior to performing an absorption measurement.

### Spectrometry

Identification of transient radicals was achieved by EPR using a Bruker EMX spectrometer. Spectra (5 scans average) were collected at room temperature at the X-Band frequency range (~9.8 GHz). Defects were further characterized by diffuse reflectance spectroscopy using a Flame-S-UV-VIS Ocean Optics® spectrometer equipped with an Ocean Optics® reflection probe R400-7-Vis/NIR at 45° (six illumination fibers and one detector) coupled with an Ocean Optics DH-2000-BAL deuterium-tungsten light source. Duplicate spectra were obtained at three different positions (120° rotations), 10 scans, 1700 ms acquisition time, and optical grade PTFE was used as a reference. The diffuse reflectance spectra were obtained by placing the probe at a distance of 2 mm from the tube surface and at a 45° angle to decrease the specular reflectance. In this way, the probe collects photons that have experienced a greater number of interactions within the material, and therefore, provide more information regarding the absorbing species. Measuring with an angle of 45 ° certainly decreases the intensity of the spectra but increasing the collection time to 1700 ms achieves optimal results.

Only relative absorbance spectra (k/s) are shown for all the analyzed systems, but each one was obtained from reflectance spectra treated with the simplified Kubelka-Munk model. The Kubelka-Munk model has proven to be an excellent approximation to convert reflectance to transmission (absorbance). Solid opaque and difficult to handle samples are often not candidates for single crystal analysis, for those, diffuse reflectance provides a viable, fast, and flexible alternative for obtaining indirectly absorbance spectra.

$$R_\infty = 1 + \frac{k}{s} - \sqrt{\frac{k}{s}\left(2 + \frac{k}{s}\right)}$$

Where $k = 4\pi\kappa/\lambda$ is the absorption coefficient of the sample, and $\lambda$ is the wavelength.

The model is based on various assumptions, for example, assumes infinite thickness of the sample (with respect to the range of photons), constant scattering regardless of the wavelength, constant packing of the sample, and uniform

particle size. The model condenses all the possible geometric peculiarities and inhomogeneity of the sample into a single parameter, the scattering coefficient "s". Therefore, the absorbance is expressed in units of absorption coefficient ($k$) over a parameter of variability "s". It is not a real unit, but the ratio k/s is proportional to the absorbance. The simplified function allows to correlate the reflectance factor to absorbance, in units dependent on the scattering coefficient, to estimate possible inhomogeneities of the sample.[34]

$$\frac{k}{s} = \frac{(1-R_\infty)^2}{2R_\infty}$$

## Results and discussion

Among alkali halides, KCl is one of the most studied systems for its ease of coloration and high extinction coefficient, which is why reflectance and EPR spectra were obtained to evaluate the reliability and repeatability of the method used.

### KCl

Radiation-induced absorption bands for the monovalent chloride crystals at room temperature can be categorized into three groups: trapped electrons (*F*, $F_2$, etc.), generally located in the visible-near IR range (400-1000 nm); trapped holes ($Cl_2^-$ and $Cl_3^-$) in the middle-near UV (200-400 nm);[12] and charged Frenkel defects ($\alpha$- and $I$-centers) in the long-wavelength tail of the fundamental band (160-200 nm). The fundamental band for $Cl^-$ is located around 160 nm for the $3p$-$4s$ excitation.[35]

The optical absorption spectra obtained through diffuse reflectance for gamma irradiated KCl are shown in Fig. 2. The absorption of *F*-centers was found at 556 nm, comparable to the values reported by Casler (560 nm) at room temperature,[36] and below 540 nm reported at low temperatures.[14, 37, 38] The shift is attributed to the effects of temperature on the volume of the crystal and changes at the electronic energy levels due to vibrations.[39]

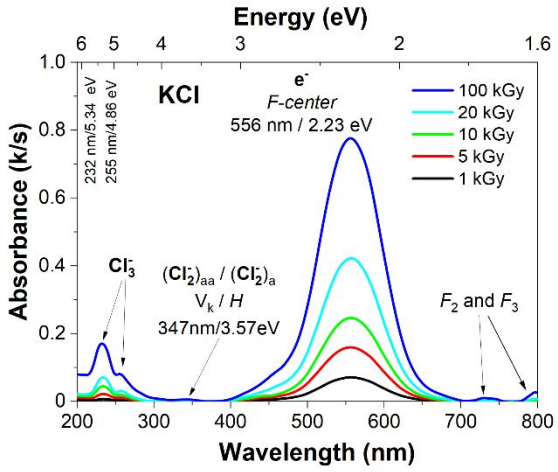


**Fig. 2.** Optical absorption spectra for gamma-irradiated KCl powders to 100 kGy absorbed gamma dose (72.4 Gy min$^{-1}$ at ~298 K) obtained through diffuse reflectance measurements (Kubelka-Munk function applied).

**Table 1**. Main absorptions detected for irradiated KCl through diffuse reflectance.

| Band name | $V_2$ | | $H$ | $V_k$ | $F$ | $F_3$ | | $F_2$ |
|---|---|---|---|---|---|---|---|---|
| Notation | $(Cl_3^-)_{aca}$ | | $(Cl_2^-)_a$ | $(Cl_2^-)_{aa}$ | $v_a^+e^-$ | $_2v_a^+e^-$ | | $_3v_a^+e^-$ |
| Wavelength (nm) | 232 | 255 | 347 | 370 | 556 | 690 | 741 | 794 |
| Energy (eV) | 5.34 | 4.86 | 3.57 | 3.35 | 2.23 | 1.79 | 1.67 | 1.56 |

Duerig and Dorendorf[15] found the $Cl_3^-$ peaks at 230 nm and 255 nm (90 K), while Sonder through electron irradiation found a broad peak shifted from 227 to 213 when raising the temperature from 80 to 274 K.[40] Faraday could not resolve the peaks and only observed a broad band at 240 nm at room temperature. The spectra obtained show agreement with the results of Duerig and Dorendorf (232 and 255 nm) despite the difference in temperatures.

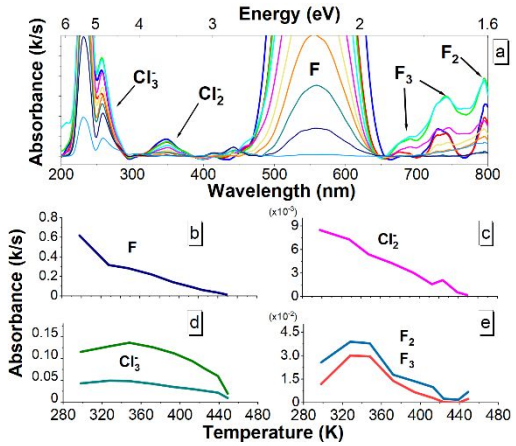


**Fig.3.** (a) Isochronous thermal bleaching curves for KCl powders irradiated at 100 kGy. (b) (c) (d) & (e) Thermal annihilation-production curves for F, $Cl_2^-$, $Cl_3^-$, $F_2$ and $F_3$ centers.

In the solid-state $Cl_2^-$ gives rise to two kind of defects, $V_k$- and *H*-centers, the difference lies in the position occupied by the chlorine atoms. While in a $V_k$-center, each chlorine atom is placed in its normal anion lattice point, i. e., the molecule occupies two anion sites $(Cl_2^-)_{aa}$;In the absorption spectrum, both centers ($V_k$ and *H*) present bands at similar wavelengths (365 nm and 336 nm, respectively),[12] corresponding to the excitation $^2\Sigma_u^+ \rightarrow {}^2\Sigma_g^+$ due to light with electric vector parallel to the molecular axis ($\sigma$),[14, 41] which cannot be completely resolved at high temperatures. In Fig.2 the peak for $Cl_2^-$ exhibited a low absorption but still observable at 347 nm (3.57 eV). Thermal bleaching showed that this band is an overlapping of two others (347 nm and 370 nm) similar to $V_k$ and *H*-centers (Fig. 3a) reported in the literature. The thermal annihilation behaviors of *F*-centers and $Cl_2^-$ showed similar rates above 320 K (Fig. 3b and Fig. 3c). In the 298-320 K range, trapped electrons start to leave anionic vacancies to migrate ($E_a$= 0.5 eV)[42] and associate with other existing *F*-centers, yielding $F_2^+$ or $F_3^+$-centers and ultimately as $F_2$ or $F_3$-centers after an electron capture. The latter is shown in Fig. 3e, reaching a maximum at 320-355 K and later decreasing at higher temperatures due to cluster disaggregation. The band at 232 nm for $Cl_3^-$ shows a slight increase, probably due to *H*-center endothermic recombination

(Fig. 3d); then undergoes disproportionation reactions to $Cl_2$ and $Cl^-$, or follows the decomposition route to produce $Cl^•$ and $Cl_2^-$ (Fig. 1).[43] The second route seems unlikely, since the increase in the 347 nm band ($Cl_2^-$) was not significant. The second band at 255 nm does not decay at the same rate as the 232 nm band, which shows enhanced stability by the interstitial ion pair perturbing the $Cl_3^-$.[44]

The well-known broad resonance line characteristic of F-centers in KCl is shown in Figure 4 for the irradiation doses performed at room temperature. The resonance line pattern consists of 19 lines from the six neighboring $K^+$ ions ($I$ = 3/2) with isotopic abundance $^{39}K$ (93.2 %) and $^{41}K$ (6.7 %); which in turn are split into 37 lines by superhyperfine interaction with 12 second-shell chloride ions ($^{35}Cl$ (75.7%) and $^{37}Cl$ (24.2%)), for an overall 703 resonance lines.[45]

At low doses (1 kGy), the peak corresponding to one component of $Cl_2^-$ ($g$ = 2.007) is barely shown, but at higher dose, the line is masked by the set corresponding to trapped electrons and lost via the instability of $Cl_2^-$ with temperature.

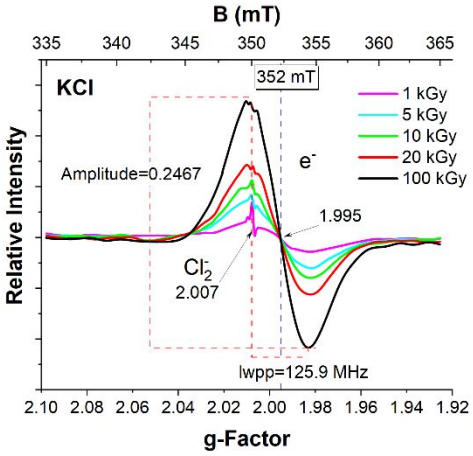


**Fig.4.** Room-temperature EPR spectra, up to 100 kGy for solid KCl (powder). Broad resonance line with g=1.995 corresponds to the overlapping of 703 absorption lines due to energy levels splitting of a trapped electron under the influence of 6 $K^+$ (hyperfine) and 12 $Cl^-$ (superhyperfine) magnetic moments. Small resonance line at low dose corresponds to $Cl_2^-$

The results obtained for KCl correspond to those reported in the literature with different irradiation and temperature conditions, which validates the reliability of the method used. The same treatment was carried out for $MgCl_2$, and $ZnCl_2$.

**$MgCl_2$**

Unlike alkali halides, alkaline earth halides are not prone to coloration quite easily. As mentioned above, the main stable radiation-induced defects are charged Frenkel-Defects ($\alpha$-$I$), not like *F*- and *H*-centers for AH.[46] After the formation of vacancies and interstitial ions, the radiation ionizes another chloride, which forms $Cl_2^-$ ($V_k$-centers), and the electron happens to occupy the vacancy just formed. Therefore, the efficiency for *F*-centers will be determined by the ease to separate the $\alpha$-$I$ defects formed (avoid recombination).[47] The temperature, packing, ion size, and possible electric fields within the crystal, are variables that lower the barriers and enhance the movement of interstitials.[46]

Previous studies have established that $Cl_2^-$ absorption peak is remarkably consistent regardless of the cation present (monovalent or divalent).[22] The spectra showed a shoulder at 354 nm which probably corresponds to $Cl_2^-$ but the EPR studies did not show the characteristic septet, hence we cannot make any conclusive statements about it. Besides *F*-centers, electrons can be trapped by divalent cations or impurities which being reduced to monovalent or ground state according to the metal, temperature, and dose. As a matter of fact, using electron traps to reduce recombination reactions is a common technique for the study of solid-state radiolysis products. For instance, Thallium forms aliovalent species ($Tl^0$, $Tl^+$, $Tl^{2+}$, or $Tl^-$) in alkali halides that absorb in the UV-Vis.[48] From these studies, it has been concluded that one of the common products in the irradiation of divalent salts is the variation of charge state of the cations.[49]

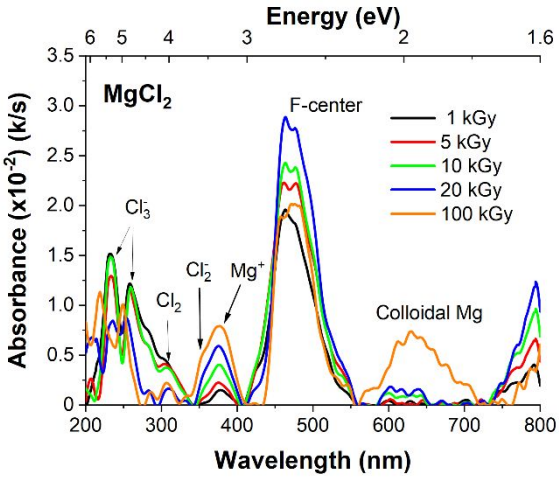


**Fig.5.** Absorption spectra for γ-irradiated $MgCl_2$ powders to 100 kGy absorbed gamma dose (298 K). Crystals reached max concentration at 10 kGy for F-centers.

The split absorption band, as observed in Fig. 5 at 462 nm (2.68 eV) and 478 nm (2.59 eV) corresponding to *F*-centers (slightly distorted), showed sustained growth until 20 kGy, followed by a 26.3% decrease at 100 kGy (Fig.6), evidence of a decrease in the Mg coordination number from the *F*-centers .[50] Confirmation of the identity of this band is provided by EPR spectra, as shown below. The double peak is most likely due to distortion of the octahedral coordination[51] and/or traces of other metals.[52] An extra peak at 378 nm (3.28 eV) increased logarithmically up to 100 kGy, apparently due to two monovalent magnesium ($Mg^{2+} + e^- \rightarrow Mg^+$) associated as M-centers. The latter might be for destruction of *F*-centers, which result in asymmetric anion vacancies and a more localized distribution of trapped electrons instead of being equally distributed between more cations. The material was not amorphized, simply the steady-state reached after 20 h of irritation caused a greater production and aggregation of defects, which changes the symmetry of the anionic vacancies, and therefore, the concentration of F-centers. Costuas et al in 2002,[50] conducted DFT studies about the strain and atom

displacement on mono an divacancies on $MgCl_2$. According to their simulations, the change in coordination induces changes in the lattice parameters of the neighboring atoms and, as a consequence, the well of potential of the vacancy. Although $Mg^+$ is not stable, clustering and association with vacancy pairs provides additional stabilization to increase the lifespan.[48] The same behavior has been reported for in divalent fluorides doped with Zn, with changing symmetries induced by radiation.[46]

In the UV region, the polyhalide multiple bands are located at 232 and 260 nm with similar intensities up to 10 kGy. Unlike the pattern shown for KCl, where the 232 nm band has a higher absorption, the increase and broadening of the 260 nm band for $MgCl_2$ confirms the overlapping of more bands due to dichroism of $Cl_3^-$ with complex geometries for the association to pairs of divalent interstitials or vacancies,[53] and the possible formation of $Cl_2$ (310 nm).[16, 54] At higher dose (>20 kGy) the pattern changes, and both bands are shifted to higher energies (219 and 249 nm) explained by stress deformations and reorientation of the molecule.[13] The shape of the doublet between 230-280 nm was also observed in the study of thermal bleaching on $ZnCl_2$.

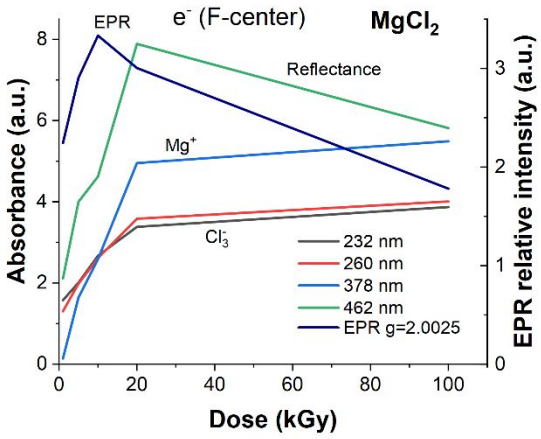


**Fig.6.** Growth curves for the main absorption bands of $MgCl_2$ crystals irradiated to 100 kGy at 298 K. The behavior of the resonance line with g = 2.025 in the EPR spectrum show coincidence with the band at 462 nm (F-center).

A wide, flat band appeared between 600-700 nm, more evident after 100 kGy absorbed dose. In alkali halides, bands like this appear at high dose and temperature, and have been related to metal colloidal defects.[55] Biggins et al (2018)[56] showed evidence that the wide band between 600-800 nm is associated with Mg nanoparticles with different dimensions. The formation of metallic Mg inside the crystal can only be explained by the presence of stable $Cl_3^-$ or by the desorption of $Cl_2$, in order to maintain the electroneutrality of the crystal structure. Magni et al. (1995), reported the desorption of $Cl_2$ in samples of $MgCl_2$ deposited on Au sheets when irradiated with electrons.[57] It is certainly a different experiment, but it shows the reduction of Mg and the formation of $Cl_2$. Gamma irradiation will produce less desorption under the experimental conditions used by us, but certainly exists. In later experiments with higher doses and amount of sample, we will conduct a study related to $Cl_2$ induced by radiation. The peak associated with $Cl_2$ decrease to minimal levels, likely due to gas diffusion out of the crystal induced by accumulated radiolytic damage at high doses.

The thermal bleaching curves (Fig. S1) showed the expected decrease in F-centers and $Mg^+$ due to recombination with $Cl_3^-$ (two $e^-$ for each trichloride), but an increase in $Cl_3^-$ as the temperature reaches 400 K, where disaggregation of clusters begins. The concentration of $Mg^+$ (M-centers) decreases when passing to the divalent state due to the loss of the captured $e^-$, but at a higher temperature it increases due to the oxidation of metallic Mg and the destruction of F-centers. It is generally accepted that the generation of color centers in alkali halides induced by low LET ionizing radiation is a reversible process. It is possible (theoretically) to regenerate the original crystal structure through heat or light treatment, though, not the case for $MgCl_2$, or at least it was not possible to recover the original absorption spectrum after 22 h above disaggregation temperature (440 K). The total disappearance of aggregates of polyhalides, $Mg^+$ or metallic Mg, was not observed.

Natural Mg is composed of 3 stable isotopes, of which only $^{25}Mg$ (10.11%) induces hyperfine splitting ($I$ = 5/2), thus, the resonance spectrum for *F*-centers with only $^{24}Mg$ and $^{26}Mg$ surrounding the anion vacancy present a single intense line; on the other hand, *F*-centers with at least one $^{25}Mg$ ion split the line into a sextet, or 11 lines if two ions are present. Despite its low abundance (10%), probabilistically, about 47% of the *F*-centers contain at least one Mg cation with a non-zero magnetic moment, as each *F*-center involves six $Mg^{2+}$ (octahedral coordination). Fig. 7 depicts EPR spectra for $MgCl_2$ powders, where the broad resonance line at $g$= 2.025 corresponds to trapped electrons (*F*-center).[58] The broadening of the peak is explained by the sharing of electron density with the 6 $Mg^{2+}$ ions surrounding the vacancy, coupled with the superhyperfine interaction from the Cl ions from the second shell, analogous to

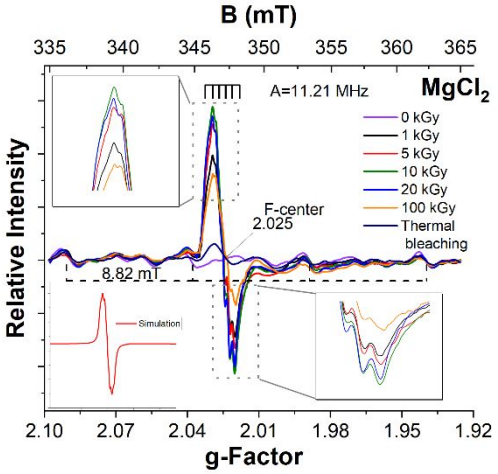


**Fig.7.** EPR spectra for $MgCl_2$ irradiated powders up to 100 kGy absorbed dose. The spectra showed resonance lines (g = 2.025) corresponding to F-centers. The inset shows the MATLAB® simulation for a system with one electron shared between six $Mg^{2+}$. The hyperfine splitting (sextuplet) is due to the presence of at least one $^{25}Mg$ surrounding the vacancy.

F-centers of octahedral alkali halides. The inset details the sextuplet induced by $^{25}Mg$ ($A$ = 11.21 MHz).

Maximum EPR signal intensity was reached at 10 kGy, followed by destruction of *F*-centers as a consequence of radiation damage. A similar trend was observed by the 462 nm band from the optical absorption spectra, which confirms its correspondence to *F*-centers (Fig. 6). Another paramagnetic center that is expected according to the absorption spectra is $Mg^+$, however if it is coupled to another $Mg^+$ the defect becomes silent to EPR. Low intensity resonance lines with A = 8.82 mT are due to traces of Mn. Its intensity does not change regardless of the dose due to its lower ionization potential with respect to Mg.

**$ZnCl_2$**

The systems previously discussed fall into the category of ionic salts with well-defined characteristics, whereas $ZnCl_2$ (melting point 290 °C) is different. $ZnCl_2$ exhibits four main crystalline arrangements of tetrahedral $Zn^{2+}$ centers that hinder the identification of defects. Due to a high second ionization potential (17.96 eV), $Zn^{2+}$ will readily trap electrons from radiation-induced ionizations to form a lower valence state ($Zn^+$), unlike some other divalent cations where transition to monovalent state, requires thermal treatment after irradiation owing to their relatively lower second ionization potential (~10 eV).[19] The main absorption features are in the UV and the beginning of the visible range (Fig. 8). We found no evidence to support the formation of F-centers, *i. e.*, the trapped electrons are not shared by several cations, but rather reduction of $Zn^{2+}$ to monovalent. At doses <20 kGy, a peak is observed at 260 nm (4.77 eV) with a shoulder at 278 nm (4.46 eV), which grows at a similar rate to that of the 365 nm band (3.36 eV) but with less intensity. The bands corresponding to $Cl_3^-$ would be expected in 236 and 260 nm (almost with the same intensity), but in the normalized spectra only the latter was observed at low doses. At a dose of 100 kGy, the missing band corresponding to $Cl_3^-$ appeared (236 nm), but thermal studies showed an accelerated decay that with only 350 K was enough to reduce it by 32%, so there must be absorption due to Zn overlapping the 236 and 260 nm peaks. In the spectrum corresponding to 100 kGy the zinc species formed can be clearly seen.

The spectrum shows 3 peaks that apparently correspond to monovalent $Zn^+$ but with different coordination. The wide Gaussian band at 365 nm (3.36 eV), presumably due to $Zn^+$ surrounded for four $Cl^-$ (high symmetry) increases with dose and overlaps with the $Cl_2^-$ band which could not be differentiated, but its presence was confirmed through the EPR spectra. The two remaining peaks at 278 nm (4.77 eV) and 236 nm (5.25 eV) would correspond to $Zn^+$ with lower coordination number plus contribution from $Cl_3^-$ as previously mentioned. Baranov et al,[59] conducted studies on Zn embedded in NaCl crystals and observed similar peaks to which he assigned as monovalent species without further details. On the other hand, articles on Zn nanoparticles have reported peaks at 232 nm and 370 nm,[60] although without conclusive analysis that confirms the oxidation state. Xiang[61] implanted Zn ions in sapphire finding a signal at 260 nm and by XPS studies, concluded correspondence to metallic zinc, showing shifts to longer wavelengths 285 nm as nanoparticle increases. It is clear that no consensus has been reached about the identity of these bands, but there is a coincidence in its correspondence to Zn.

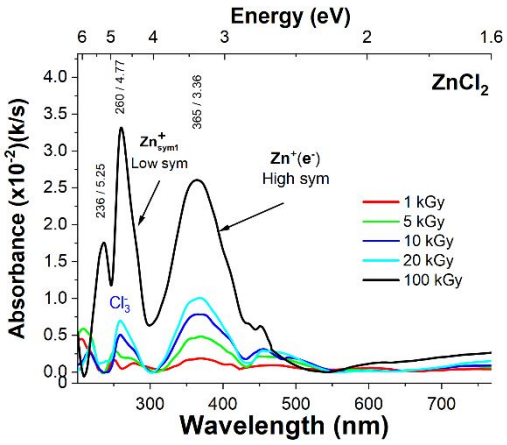


**Fig.8.** Absorption spectra for $ZnCl_2$ salts irradiated to 100 kGy at room temperature. At a dose of 100 kGy, species with monovalent zinc centers with different geometries were detected.

The trend followed by the peaks can be explained by the higher abundance of vacancies and interstitials. In symmetric paramagnetic centers ($Zn^+_{365nm}$), the $Zn^+$ (trapped electron) is surrounded by four $Cl^-$ ions, when one of them is displaced, the coordination (and symmetry) is modified, and with it, the absorption intensity. Below 20 kGy only $Zn^+$ are observed with 2 different symmetries (365 nm and 260 nm) but at 100 kGy a third symmetry appears at (236 nm). This pattern has been reported, although in other types of salts.[46] The position of the bands is not the same, but a model that implies the disruption of symmetry due to radiation, and subsequent growth of absorption bands with less symmetry, seems to be applicable.

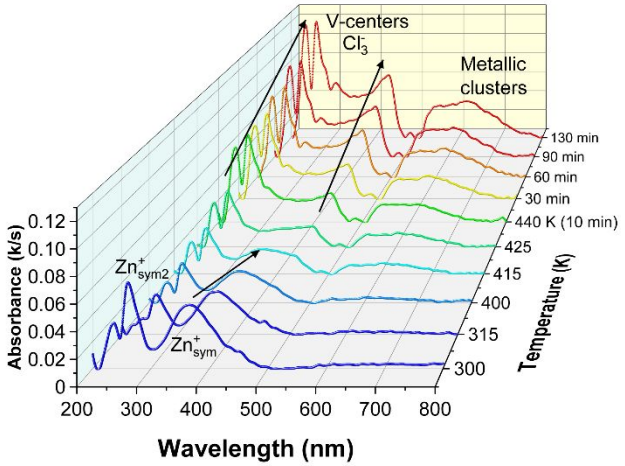


**Fig.9.** Thermal bleaching of $ZnCl_2$ salts irradiated to 100 kGy. Heating causes the formation of metal clusters and dislocation loop aggregates.

The thermal bleaching curves (Fig. 9) showed changes in the absorbance of the peaks which can be explained by the diffusion of interstitial ions to form aggregates (dislocation loops), and complimentary Zn metallic clusters.[27] The decrease in the 236, 260, and 365 nm peaks due to $Zn^+$, agrees with the

growth of the 600-700 nm band ($Zn^0$) up to 425 K. Upon reaching 440 K, no presence of 365 nm band is observed, and 236/260 nm peaks reach a minimum. At the mentioned temperature, the isothermal study was carried out increasing heating time, and the peaks at 236 nm and 260 nm began to grow, but not due to the presence of $Zn^+$ but for the formation of halide aggregates. Similarly, the flattened band associated with metallic Zn continued to grow at the same rate as the peaks at 236 and 260 nm. The 3 mentioned species can be visualized as follows:

$$Zn^+ + e^- \rightarrow Zn^0 \quad \text{600-700 nm}$$

$$Cl_i^{\cdot} + Cl_i^{\cdot} \rightarrow Cl_2 \text{ (interstitial)} \quad \text{310 nm}$$

$$Cl_2 + Cl^- \rightarrow Cl_3^- \text{ (dislocation loops)} \quad \text{236 and 260 nm}$$

Finally, the band around 310 nm, presumably for $Cl_2$ trapped in interstitials, grows, and a new peak begins to appear at 430 nm (2.87 eV), probably associated with Zn metal clusters.

The EPR spectra (Fig. 10) provide resolved evidence for two different types of radicals: electrons trapped by $Zn^{2+}$ and $Cl_2^-$. The resonance line for $Zn^+$ has a sharp, resolved signal indicating a localized trapped electron, unlike the resonance line shown in Fig. 7 for $MgCl_2$ (delocalization of charge). It is interesting to observe $Cl_2^-$ in powders irradiated at room temperature since its presence has been reported only at low temperatures,[21] but the signal disappears during annealing. The $Cl_2^-$ radical is not commonly associated with vacancies ($V_F$-center)[3] or impurities, however, its concentration increases when electron traps (such as divalent cations with high ionization potential) are present, as in the current case. Undoubtedly, the crystalline structure and the high ionization potential of Zn diminish recombination, enhance the separation of *F-H* pairs, but not to the extent to allow complete halide aggregation. Most of the trapped holes will be found in halide aggregates as shown by the absorption spectra, but EPR shows some isolated $Cl_2^-$.

The set of resonance lines centered at g= 2.063 corresponds to electrons trapped by $Zn^{2+}$ cations turning to monovalent ($Zn^+$). Natural Zn is composed of 5 isotopes, but only $^{67}Zn$ (4%) has a non-zero nuclear spin, so a low-intensity sextuplet flanks the main lines (satellites). An isotropic signal would be expected for the trapped electrons; however, as explained in the previous section, changes in symmetry due to radiation damage generate anisotropy. A more detailed look of the signal (inset in

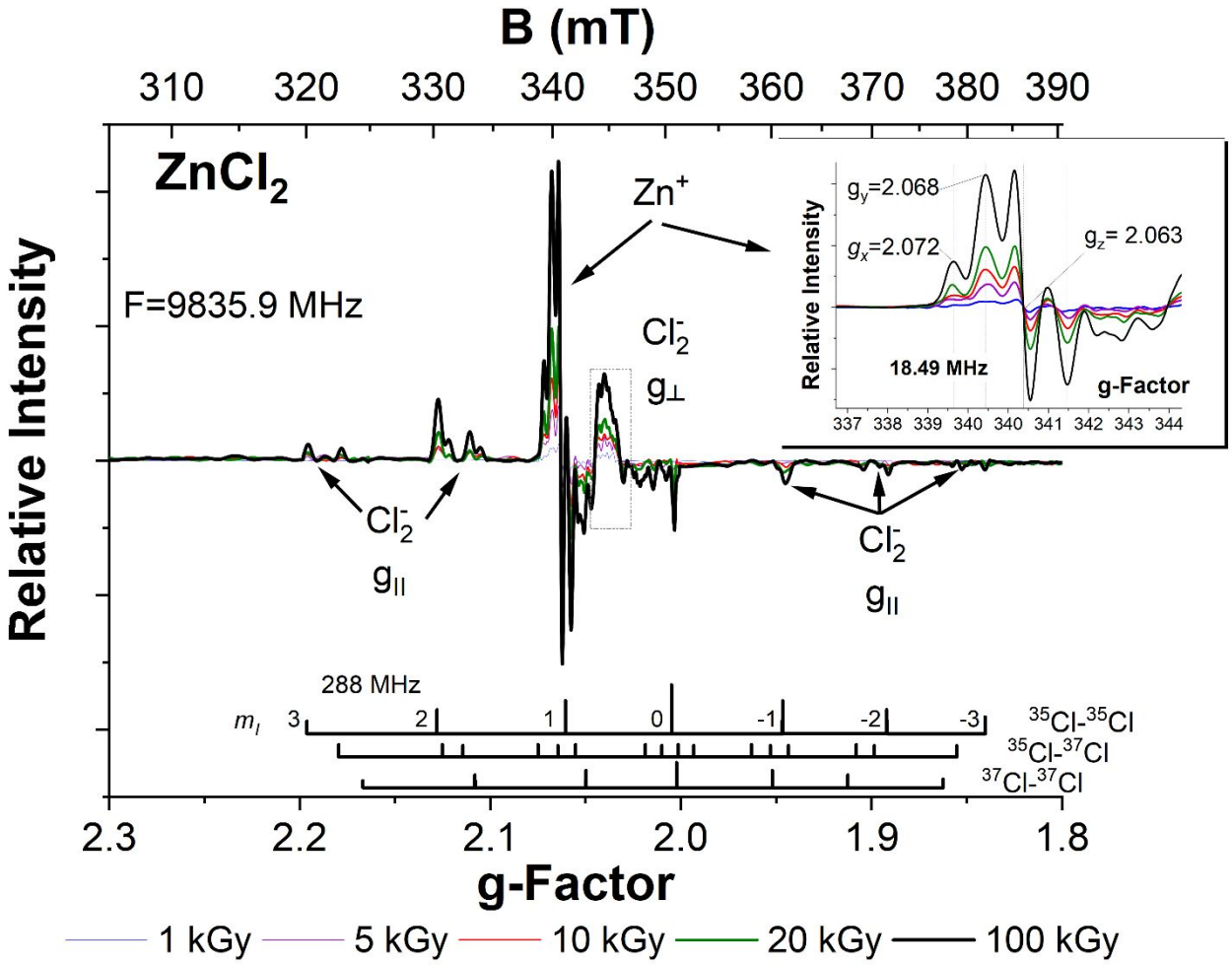


**Fig. 10**. EPR spectra for $ZnCl_2$ irradiated to 100 kGy absorbed gamma dose. The spectrum shows the characteristic lines of monovalent $Zn^+$ and $Cl_2^-$. Inset. Magnified signal for electrons captured by $Zn^{2+}$. The $Cl_2^-$ spectrum appears as a low intensity septuplet for centers parallel to the field and as an unresolved signal for centers perpendicular to the field (g = 2.044).

Figure 10) shows three lines ($g_x$= 2.072; $g_y$=2.068 and $g_z$=2.063) with A = 18.49 ± 0.12 MHz.

The pattern for $Cl_2^-$ is more complex. The spectrum in single crystals is composed of 7 signals almost equally spaced with relative intensities 1: 2: 3: 4: 3: 2: 1, corresponding to one electron (or the lack of one from the "hole" standpoint) shared between two Cl nuclei with $I$ = 3/2, resulting in a system with total nuclear magnetic quantum number ($m_I$) with 3, 2, 1, 0, -1, -2 and -3 possible values. The existence of two main stable isotopes of Cl, with slightly different magnetic moments ($\gamma^{37}/\gamma^{35}$ = 0.832)[62] and non-zero nuclear spins, split the septuplet system to a more complex pattern of 29 lines for the 3 possible isotopologues: ($^{35}Cl$-$^{35}Cl$)$^-$, ($^{35}Cl$-$^{37}Cl$)$^-$ and ($^{37}Cl$-$^{37}Cl$)$^-$.[45] The dichloride anion is a linear molecule so it should present axial symmetry; however, the spectrum showed g-factor anisotropy (rhombic) and axial A-tensor. The anisotropy generated by said symmetry, the different magnetic moments of the chlorine isotopes, and the orientations of the molecular radical ion inside the crystal, result in spectra with different intensities, hyperfine splitting and shifting of the center line; however, the septuplet pattern is conserved. The combination or overlap of all these spectra is what is observed when analyzing powders, but two main orientations present the higher resonance lines, the $Cl_2^-$ parallel ($g_\parallel$), and the perpendicular $g_\perp$ to the magnetic field.

The resonance lines for magnetic centers parallel to the field showed signals at 320.04, 330.34, 340.64, 350.94, 361.24, 371.54 and 381.85 mT, with a central value of $g_\parallel$= 2.001 and A = 288 MHz for $^{35}Cl$-$^{35}Cl$. The signal for perpendicular centers showed a broad, unresolved line with a central value of $g_\perp$= 2.044. Its intensity is higher by probability distribution (there are fewer crystals oriented parallel to the field than perpendicular).

## Conclusions

The results showed that the use of diffuse reflectance, coupled with EPR studies, provides reproducible and reliable information for the determination of long-lived transients and diffusion-promoted aggregates on irradiated potassium, magnesium, and zinc chlorides at room temperature. All three systems yielded radiation-induced defects consisting of trapped holes (polyhalides) with remarkably similar absorption profiles in terms of shape and energy, especially for salts with the divalent cations ($Mg^{2+}$ and $Zn^{2+}$). The slight shifts in absorption are explained by differences in geometry and lattice energy, in addition to the dichroism that has been reported for $Cl_3^-$. The temperature for thermal disaggregation of polyhalides increased from $K^+$< $Mg^{2+}$< $Zn^{2+}$, apparently related to the ionization potential of the cation present.

In the case of $MgCl_2$, experimental evidence for the presence of F-centers and monovalent $Mg^+$ (M-centers) was found. The stability of these centers is lower relative to KCl showing max absorption at 20 kGy, which suggests that for similar coordinations the stability of F-centers with divalent cations is lower. Unlike $MgCl_2$, $ZnCl_2$ did not show the presence of F-centers, suggesting that a higher ionization potential (and lower coordination number) impacts the stability of the trapped electrons. In $ZnCl_2$, the presence of monovalent cations with different coordination geometries was observed, although studies and simulations are required to determine their identity. In addition, the irradiated salts showed the presence of trapped $Cl_2^-$ at room temperature irradiation and measured 3 min after irradiation, which had only been reported at low temperatures in solids and measurements in-situ. The studies of thermal bleaching in $ZnCl_2$ showed the progressive formation of metallic clusters with increasing heating time. Thermal studies showed that temperature promotes diffusion, and consequently, secondary processes, increasing the concentration of polyhalides and regions with a high concentration of cations in the divalent salts. This was not the case for KCl, since the absorption of the defects progressively decreases until it disappears. The results suggest that the ionization potential is decisive in the speciation of the initial radiation-induced transients, and that the coordination geometry impacts the depth of the potential well for trapping and stabilization of electrons, even at high temperatures.

## Conflicts of interest

There are no conflicts to declare.

## Acknowledgements

This work was supported as part of the Molten Salts in Extreme Environments (MSEE), an Energy Frontier Research Center, funded by the U.S. Department of Energy (DOE), Office of Science, Basic Energy Sciences (BES) at the University of Notre Dame under award DE-FC02-04ER15533, at Brookhaven National Laboratory under contract DE-SC0012704 and at Idaho National Laboratory under contract DE-AC07-05ID14517.

MSEE work at the University of Notre Dame is funded under subcontract to Brookhaven National Laboratory. The authors thank Phillip Halstenberg and Sheng Dai at University of Tennessee, Knoxville, for the distillation of $ZnCl_2$ and $MgCl_2$ salt samples, and William C. Phillips at Idaho National Laboratory for his assistance with the preparation of initial batches of samples. The authors thank Prof. Ian Carmichael for making available the facilities of the Notre Dame Radiation Laboratory. This contribution is NDRL-5305 from the Notre Dame Radiation Laboratory.

## References

1. K. Beierschmitt, M. Buchanan, A. Clark, I. Robertson, P. Britt, A. Navrotsky, P. Burns, P. Tortorelli, A. Misra, J. Wishart, P. Fenter, A. Gewirth, B. Wirth, B. Mincher, I. Szlufarska, J. Busby, L. Horton, B. Garrett, J. Vetrano, P. Wilk, K. Runkles, S. Kung, S. Lesica, B. Wyatt, D. Counce and K. Jones, *Basic Research Needs for Future Nuclear Energy: Report of the Basic Energy Sciences Workshop for Future Nuclear Energy, August 9-11, 2017*, U.S.Department of Energy. Office of Science, USA, 2017.

2. D. F. Williams and P. F. Britt, *Technology and Applied R&D Needs for Molten Salt Chemistry:Innovative Approaches to Accelerate Molten Salt Reactor Development and Deployment*, U.S. Department of Energy, Tennessee, 2017.
3. A. Lushchik, C. Lushchik, E. Vasil'chenko and A. I. Popov, *Low Temperature Physics*, 2018, **44**, 269-277.
4. S. J. Black and D. M. J. Compton, *The Journal of Physical Chemistry*, 1965, **69**, 4421-4422.
5. A. K. Pikaev, I. E. Makarov and T. N. Zhukova, *Radiat Phys Chem*, 1982, **19**, 377-387.
6. R. Casler, P. Pringsheim and P. Yuster, *J Chem Phys*, 1950, **18**, 887-891.
7. Z. P. Zagorski, *Radiat Phys Chem*, 1999, **56**, 559-565.
8. W. R. Grimes, *Nuclear Applications & Technology*, 1970, **8**, 137-155.
9. M. A. Mussaeva, E. M. Ibragimova, M. U. Kalanov and M. I. Muminov, *Phys Solid State+*, 2006, **48**, 2295-2299.
10. J. D. Konitzer and H. N. Hersh, *J Phys Chem Solids*, 1966, **27**, 771-781.
11. H. N. Hersh, *Phys Rev*, 1957, **105**, 1158-1167.
12. C. J. Delbecq, P. H. Yuster and W. Hayes, *Phys Rev*, 1961, **121**, 1043-1050.
13. C. D. Clark and D. H. Newman, *J Phys Part C Solid*, 1971, **4**, 1130-1144.
14. C. J. Delbecq, B. Smaller and P. H. Yuster, *Phys Rev*, 1958, **111**, 1235-1240.
15. H. Dorendorf, *Zeitschrift für Physik*, 1951, **129**, 317-326.
16. S. Hubinger and J. B. Nee, *J Photoch Photobio A*, 1995, **86**, 1-7.
17. P. W. Levy, *J Phys Chem Solids*, 1991, **52**, 319-349.
18. V. I. Dubinko, A. A. Turkin, D. I. Vainshtein and H. W. den Hartog, *Nucl Instrum Meth B*, 2000, **166**, 561-567.
19. S. Radhakrishna and B. V. R. Chowdari, *physica status solidi (a)*, 1972, **14**, 11-39.
20. J. D. Comins and P. T. Wedepohl, *Solid State Commun*, 1966, **4**, 537-540.
21. T. G. Castner and W. Kanzig, *J Phys Chem Solids*, 1957, **3**, 178-195.
22. M. N. Kabler, in *Point Defects in Solids: General and Ionic Crystals*, eds. J. H. Crawford and L. M. Slifkin, Springer US, Boston, MA, 1972, DOI: 10.1007/978-1-4684-2970-1_6, ch. 6, pp. 327-380.
23. *Defects and Their Structure in Nonmetallic Solids*, Springer US, USA, 1 edn., 1976.
24. A. V. Egranov, E. A. Radzhabov, A. I. Nepomnyashchikh, V. F. Ivashechkin and I. E. Vasil'eva, *Phys Solid State+*, 2008, **50**, 1740-1746.
25. A. Dauletbekova, F. Abuova, A. Akilbekov, E. Kotomin and S. Piskunov, *Phys Status Solidi C*, 2013, **10**, 160-164.
26. A. E. Hughes and S. C. Jain, *Advances in Physics*, 1979, **28**, 717-828.
27. L. W. Hobbs, A. E. Hughes and D. Pooley, *Proceedings of the Royal Society of London. Series A, Mathematical and Physical Sciences*, 1973, **332**, 167-185.
28. W. A. Sibley and O. E. Facey, *Phys Rev*, 1968, **174**, 1076-&.
29. M. Nakagawa, M. Okada, K. Atobe, H. Itoh, S. Nakanishi and K. Kondo, *Radiation Effects and Defects in Solids*, 1991, **119-121**, 663-668.
30. S. Kinno and R. Onaka, *J Phys Soc Jpn*, 1983, **52**, 267-271.
31. C. T. Butler, Doctor of Philosophy, Oklahoma State University, 1972.
32. F. Wu, S. Roy, A. S. Ivanov, S. K. Gill, M. Topsakal, E. Dooryhee, M. Abeykoon, G. Kwon, L. C. Gallington, P. Halstenberg, B. Layne, Y. Ishii, S. M. Mahurin, S. Dai, V. S. Bryantsev and C. J. Margulis, *J Phys Chem Lett*, 2019, **10**, 7603-7610.
33. H. Fricke and E. J. Hart, *J Chem Phys*, 1935, **3**, 60-61.
34. M. L. Myrick, M. N. Simcock, M. Baranowski, H. Brooke, S. L. Morgan and J. N. McCutcheon, *Appl Spectrosc Rev*, 2011, **46**, 140-165.
35. P. L. Hartman, J. R. Nelson and J. G. Siegfried, *Phys Rev*, 1957, **105**, 123-130.
36. R. Casler, P. Pringsheim and P. Yuster, *J Chem Phys*, 1950, **18**, 1564-1571.
37. B. J. Faraday and W. D. Compton, *Phys Rev*, 1965, **138**, A893-A911.
38. W. H. Duerig and J. J. Markham, *Phys Rev*, 1952, **88**, 1043-1049.
39. R. K. Dawson and D. Pooley, *Phys Status Solidi*, 1969, **35**, 95-105.
40. E. Sonder, W. A. Sibley, J. E. Rowe and C. M. Nelson, *Phys Rev*, 1967, **153**, 1000-1008.
41. *Electron Paramagnetic Resonance: A Practitioner's Toolkit*, John Wiley & Sons, Inc., USA, 1 edn., 2009.
42. F. C. Brown, in *Point Defects in Solids: General and Ionic Crystals*, eds. J. H. Crawford and L. M. Slifkin, Springer US, Boston, MA, 1972, DOI: 10.1007/978-1-4684-2970-1_8, ch. 8, pp. 491-549.
43. C. Lushchik, R. I. Gindina, A. A. Maaroos, L. A. Ploom, A. Lushchik, L. Pung, Y. V. Pyllusaar and K. A. Soovik, *Phys Solid State+*, 1977, **19**, 2117-2120.
44. C. Lushchik, A. Elango, R. Gindina, L. Pung, A. Lushchik, A. Maaroos, T. Nurakhmetov and L. Ploom, *Semiconductors and insulators*, 1980, **5**, 133-152.
45. M. Chiesa and E. Giamello, in *Electron Paramagnetic Resonance. A Practitioner's toolkit*, eds. M. Brustolon and E. Giamello, John Wiley & Sons, Inc, USA, 2009, DOI: 10.1002/9780470432235.ch13, ch. 13, pp. 489-510.
46. A. V. Egranov, E. A. Radzhabov, V. F. Ivashechkin, M. A. Semenova and I. E. Vasil'eva, *J Phys-Condens Mat*, 2008, **20**.
47. E. Kotomin, V. Kuzovkov, A. I. Popov, J. Maier and R. Vila, *J Phys Chem A*, 2018, **122**, 28-32.
48. T. Tsuboi, *Can J Phys*, 1979, **57**, 1510-1515.
49. A. I. Popov, E. A. Kotomin and J. Maier, *Nucl Instrum Meth B*, 2010, **268**, 3084-3089.
50. K. Costuas and M. Parrinello, *Journal of Physical Chemistry B*, 2002, **106**, 4477-4481.
51. A. Dauletbekova, K. Schwartz, M. V. Sorokin, J. Maniks, A. Rusakova, M. Koloberdin, A. Akilbekov and M. Zdorovets, *Nucl Instrum Meth B*, 2013, **295**, 89-93.
52. D. E. Partin and M. Okeeffe, *J Solid State Chem*, 1991, **95**, 176-183.
53. E. M. Winter, D. R. Wolfe and R. W. Christy, *Phys Rev*, 1969, **186**, 949-952.
54. W. J. Soppe, H. Donker, A. G. Celma and J. Prij, *J Nucl Mater*, 1994, **217**, 1-31.
55. A. E. Hughes and S. C. Jain, *Advances in Physics*, 1979, **28**, 717-828.
56. J. S. Biggins, S. Yazdi and E. Ringe, *Nano Lett*, 2018, **18**, 3752-3758.
57. E. Magni and G. A. Somorjai, *Surf Sci*, 1995, **341**, L1078-L1084.

 

58. J. E. Wertz, P. Auzins, R. A. Weeks and R. H. Silsbee, *Phys Rev*, 1957, **107**, 1535-1537.
59. P. G. Baranov, R. A. Zhitnikov and V. A. Khramtsov, *Phys. Status Solidi (b); (German Democratic Republic)*, 1978, **86**, K67-K70.
60. S. Singh and R. Gopal, *Bulletin of Materials Science*, 2007, **30**, 291-293.
61. X. Xiang, X. T. Zu, S. Zhu, C. F. Zhang and L. M. Wang, *Nuclear Instruments and Methods in Physics Research Section B: Beam Interactions with Materials and Atoms*, 2006, **250**, 192-195.
62. N. J. Stone, *Atom Data Nucl Data*, 2005, **90**, 75-176.